ACS APPLIED MATERIALS & INTERFACES

Research Article

www.acsami.org

Radiation Sensors Based on the Generation of Mobile Protons in Organic Dielectrics

Eleftherios Kapetanakis,*[,†,‡] Antonios M. Douvas,[‡] Panagiotis Argitis,[‡] and Pascal Normand[‡]

[†]Department of Electronics, Technological Educational Institute of Crete, 73133 Chania, Greece

[‡]Department of Microelectronics, NCSR "Demokritos," 15310 Aghia Paraskevi, Greece

ABSTRACT: A sensing scheme based on mobile protons generated by radiation, including ionizing radiation (IonR), in organic gate dielectrics is investigated for the development of metal−insulator−semiconductor (MIS)-type dosimeters. Application of an electric field to the gate dielectric moves the protons and thereby alters the flat band voltage (V_{FB}) of the MIS device. The shift in the V_{FB} is proportional to the IonR-generated protons and, therefore, to the IonR total dose. Triphenylsulfonium nonaflate (TPSNF) photoacid generator (PAG)-containing poly(methyl methacrylate) (PMMA) polymeric films was selected as radiation-sensitive gate dielectrics. The effects of UV (249 nm) and gamma (Co-60) irradiations on the high-frequency capacitance versus the gate voltage ($C-V_G$) curves of the MIS devices were investigated for different total dose values. Systematic improvements in sensitivity can be accomplished by increasing the concentration of the TPSNF molecules embedded in the polymeric matrix.

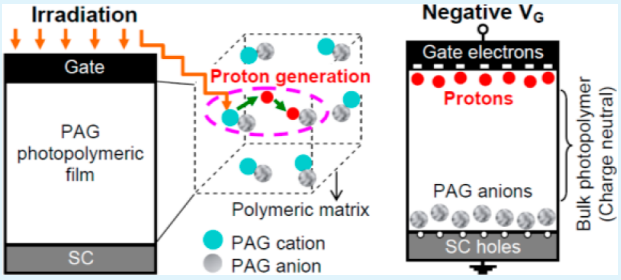

KEYWORDS: *photoacid generator, organic electronics, metal−insulator-semiconductor capacitor, field effect devices, dosimeter, radiation sensor*

1. INTRODUCTION

Ionizing radiation (IonR) has practical applications in many areas such as nuclear science, medicine, metallurgy, the food industry, and the environment. For most applications and personal safety concerns, accurate monitoring and control of the radiation dose is necessary. Depending on the radiation type and dose level to be detected, a wide variety of radiation detection and measurement devices have been developed,[1] including mainly the ionization chambers, scintillation, and thermoluminescent detectors as well as film badge dosimeters and semiconductor detectors. The latter are in the form of silicon (or germanium) diodes or metal-oxide-semiconductor (MOS)-field-effect-transistors (FETs). In addition to their low power requirement, low cost, small size, and electronic output signal, the MOS sensors can be employed for real-time monitoring of the radiation dose. They are the most commonly used solid-state integrating dosimeters[2] with applications in various fields ranging from space exploration to nuclear facilities, high-energy physics laboratories, clinical environments (radiotherapy), and the homeland security domain.[3−6] The operating principle of MOS sensors is based on the threshold voltage shift of a MOSFET caused by radiation-induced generation of positive charges (holes) in the gate oxide. The threshold voltage shift is proportional to the radiation dose. MOS sensors' sensitivity is strongly dependent on the gate oxide thickness, thus requiring large bias voltages to efficiently separate and collect the ionized charges.[7] This limits their applications to situations in which such voltages are easily available. While the choice of a radiation dosimeter is situation dependent, there is a growing demand for integrating microdosimeters that are accurate, sensitive, portable, flexible, mechanically robust, able to give online reading, and inexpensive.[8−19]

In this paper, we report a new sensing scheme that is based on the concept of radiation-induced generation of protons in photoacid-generator (PAG)-containing polymeric gate dielectrics of metal−insulator−semiconductor (MIS)-type devices. Radiation detection systems based on acid generation in solutions or polymeric films containing both a PAG and an acid-sensitive dye, where the generated acid was detected by the color change of the dye, have been reported for the development of γ-ray film dosimeters.[20,21] However, the concept of using polymeric films with embedded PAG molecules as radiation-sensitive gate dielectrics of MIS devices, wherein proton generation as a function of the IonR dose is electronically sensed,[22] is fundamentally different from the above ones and has not been explored for the realization of a MIS-type dosimeter.

The aimed ionizing radiation (IonR) sensor might be mostly understood through Figure 1, which depicts a schematic of a MIS capacitor made by sandwiching a PAG-embedded photopolymeric layer between two electrodes made of semiconductor (SC) and metal materials. The PAG is an ionic salt consisting of a sulfonium cation, responsible for the

Received: March 19, 2013
Accepted: May 22, 2013
Published: May 22, 2013

   dx.doi.org/10.1021/am401016n | ACS Appl. Mater. Interfaces 2013, 5, 5667−5674

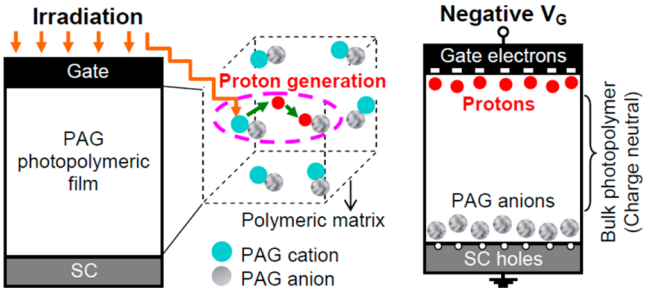

Figure 1. (Left) MIS capacitor made by sandwiching a PAG-embedded photopolymeric layer between two electrodes of semiconductor, SC, and metal materials. (Center) PAG cation responsible for the absorption of radiation and generation of protons. (Right) Operation principle of a MIS radiation sensor device.

absorption of UV radiation and generation of Brönsted acid, and a hydrophobic sulfonate anion. The photochemical generation of Brönsted acid by triarylsulfonium salts was initially proposed for the photoinitiation of cationic polymerization,[23,24] but it found wide application in the chemically amplified resists in photolithography.[25] In these resists usually employed for sub-500 nm structures, the triarylsulfonium salt based PAG generates Brönsted acid upon optical, e-beam, or X-ray irradiation of the resist film, which subsequently catalyzes or initiates the necessary for solubility change chemical reactions.[26] It has recently been proposed to use sulfonium salts as a class of organic ionic compound elements in organic light emitting diode technology[27] with attractive characteristics that can improve charge injection in polymer light emitting devices.[28]

The operating principle of the MIS-type IonR-device exploits the fact that the generated protons upon ionizing irradiation in the polymeric gate insulator can be moved by biasing the gate terminal.[22] The motion of protons at either side of the photopolymeric gate dielectric depends on the direction of the applied electric field. For example, a negative bias (V_G) applied to the gate electrode moves the photochemically generated protons to the gate/PAG-polymeric layer interface, while leaving the counter PAG anions close to the SC/PAG-polymeric layer interface, which in return attracts positive charges (i.e., holes) from the semiconductor. No spatial distribution of ionic charges occurs in the bulk of the PAG-polymeric layer, as each proton stays close to its counterion forming a neutral acid molecule. This electric-field assisted transfer of protons shifts the flat-band voltage of the MIS device as compared to proton free devices (i.e., to nonirradiated devices). The change in flat-band voltage is not only electric-field direction dependent, a trait which confers bistability to the devices, but also is proportional to the amount of IonR-generated protons and, therefore, to the IonR dose. To ensure proper operation of the above sensing scheme, the following requirements need to be met: (a) The capacitor electrodes should be made from ion-blocking materials. (b) The polymeric matrix must be an electrically insulating layer (for acting as gate dielectric) which allows the motion of protons. (c) The base polymer must not react with acids (at relatively low temperatures), and its electrical properties should not be affected from the ionizing radiation. (d) The PAG should generate quite easily protons photochemically.

2. RESULTS AND DISCUSSION

Poly(methyl methacrylate) (PMMA) was selected as the polymer matrix, because it is chemically inert at relatively high concentrations of photogenerated acid. Triphenylsulfonium nonaflate (TPSNF) was selected as the PAG, because it generates strong Brönsted acid upon DUV and gamma irradiation and is stable at high temperatures (~200 °C). The fluorinated sulfonate anion is used to increase the acidity of the generated acid and also to generate uniform distribution of PAG molecules within a more hydrophobic polymeric matrix. The MIS device structure consists of a TPSNF−PMMA layer with a physical thickness of about 270 nm sandwiched between a 12-nm-thick Al metal gate electrode and an n-type silicon substrate with a 7.5-nm-thick oxide layer on top. The use of an oxide layer gives excellent Si/SiO_2 interface properties, thus avoiding interface related capacitance distortions. The PAG−polymer layer is incorporated by spin coating of PMMA solutions containing TPSNF in various contents. The Al gate electrode was selected to be very thin in order to be semitransparent to subsequent deep UV exposure.

The Effects of UV Irradiation on the Characteristics of n-Type Si MIS Capacitors. The bistable behavior of a MIS device using a TPSNF−PMMA layer as a gate dielectric after UV exposure is evidenced by the hysteresis loops of the high-frequency (HF, 1 MHz) capacitance versus the gate voltage ($C-V_G$) curves and the corresponding shifts in the flat-band voltage (V_{FB}) shown in Figure 2a and b, respectively. The

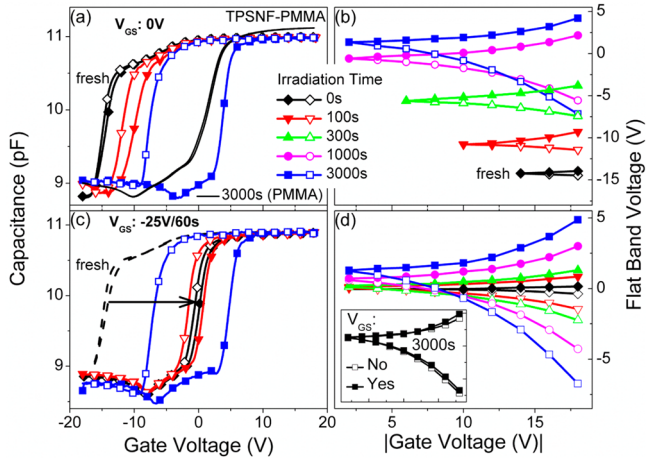

Figure 2. $C-V_G$ characteristics (a and c) and respective extracted flat-band voltages (b and d) of Al/TPSNF−PMMA/SiO_2/*n*-Si MIS capacitors after exposure to UV light. (a and b and c and d refer to the unstressed and high negative voltage stressed (V_{GS}) capacitors, respectively. (Inset) $V_{FB}-V_G$ characteristics of an unstressed and stressed device after prolonged illumination time.

TPSNF−PMMA layer was prepared from a solution containing PMMA (5% w/w in solution) and TPSNF (5% w/w in polymer) using methyl isobutyl ketone (MIBK) as a solvent. The $C-V_G$ curves were recorded under ambient and dark conditions by applying to the Al gate electrode different symmetric forward (closed symbols) and backward (open symbols) round voltage sweeps with a voltage step of 0.2 V/s, i.e., by sweeping V_G from inversion ($-V_G$), from −2 V to −18 V with the interval of −2 V, to accumulation ($+V_G$) and back to inversion. V_{FB} was defined as the gate voltage corresponding to $C/C_{max} = 0.9$, where the maximum measured capacitance, C_{max}, is the accumulation region capacitance. The "fresh" $C-V_G$ and

dx.doi.org/10.1021/am401016n | ACS Appl. Mater. Interfaces 2013, 5, 5667−5674

$V_{FB}-V_G$ curves refer to the unstressed and nonirradiated MIS capacitor, respectively. The "fresh" capacitor shows a negative flat-band voltage of −14.5 V and does not exhibit any appreciable shift in the $C-V_G$ characteristics even at high gate voltages (Figure 2a).

Upon subsequent irradiation with 249 nm light, the $C-V_G$ curves display for low forward/backward V_G sweeps a nonhysteretic behavior but drift toward the positive direction of the gate bias (right shift) with increasing irradiation time, an interesting trait which will be discussed in more detail below. Application of higher forward/backward V_G sweeps shifts the $C-V_G$ curves in the positive/negative direction of the gate bias; the higher the negative/positive gate voltage ($-V_G/+V_G$), the higher the flat-band voltage shift (ΔV_{FB}). For a given forward/backward V_G sweep, ΔV_{FB} increases with increasing the capacitor's irradiation time (Figure 2b). The hysteresis in the $C-V_G$ curves is attributed to the mobile protons generated photochemically upon irradiation of the TPSNF−PMMA layer.

Monitoring of Photoacid Generation with an Acid Indicator. The photogenerated acid within the TPSNF−PMMA films was detected with UV spectroscopy by monitoring the protonation of a suitable acid indicator, 1-(4′-(dimethyl-aminophenyl)-6-phenyl-1,3,5-hexatriene (DMADPH) introduced in those films in a 1:1 molar ratio in relation to TPSNF salt (see Figure 3). The TPS−DMADPH−

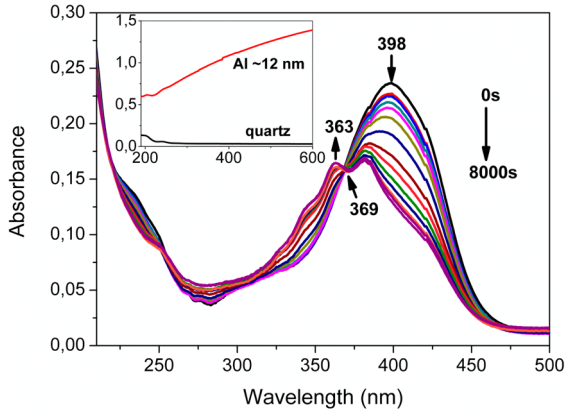

Figure 3. UV monitoring of photogenerated acid (within TPSNF−PMMA film) with the use of acid indicator DMADPH. Inset: a quartz slide covered with a 12-nm-thick Al layer used as an additional filter to the 249 nm narrow band filter, for the UV irradiation of the TPSNF−DMADPH−PMMA film.

PMMA film was exposed to UV light through both a 249 nm narrow band filter and a quartz slide covered with a 12-nm-thick Al layer ($A_{249} \sim 0.7$), i.e. in the UV exposure conditions of the MIS device. As shown in Figure 3, the photogenerated (by TPSNF) acid causes a progressive decrease in the main peak of DMADPH at 398 nm and a large shift of that band at lower wavelength (363 nm). Also, an isosbestic point at 369 nm appears, indicating that no intermediates are involved during the protonation of DMADPH. The large shift of the absorption peak of the dye due to its protonation (see Scheme 1) is caused by the extended charge delocalization in the highly conjugated system of the molecule.[29]

In a manner similar to that described in Figure 1, a negative/positive voltage causes the mobile protons to accumulate close to the upper/lower edge of the TPSNF−PMMA layer. This accumulation of protons produces two distinct spatial

Scheme 1. Protonation of DMADPH

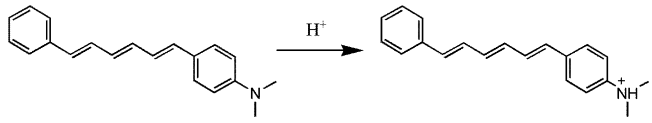

distributions of ionic charges across the TPSNF−PMMA layer that screen the gate potential and modulate the silicon substrate conductivity in a region close to the Si/SiO_2 interface. In other words, such distributions shift the flat-band voltage to more positive or more negative values, so that the MIS device switches between two well distinguishable capacitive states. The presence of mobile ions in the PMMA matrix (a general drawback of polymeric gate dielectric materials[30]) has been ruled-out, as the reference MIS devices using a spin-coated PMMA layer of thickness similar to that of the TPSNF−PMMA layer do not exhibit any appreciable shift in the $C-V_G$ characteristics even at high gate voltages after a prolonged irradiation time period of 50 min (Figure 2a).

***C*−*V*$_G$ Measurements after the Application of High Negative Voltage Stress.** The large negative V_{FB} value of the "fresh" capacitor reveals the existence of positive charges trapped within the gate insulator in a region close to the silicon substrate. For an ideal dielectric, there should be no trapped charges, and as a result the flat-band voltage should be zero[31] (if we neglect the work function difference between aluminum and silicon). The presence of such positive charges in the SiO_2 layer or/and at the Si/SiO_2 interface or in the PMMA layer or/and at the SiO_2/PMMA interface have been ruled out, as the reference MIS devices do not exhibit significant V_{FB} departure from what is expected for charge free dielectrics. It is assumed that the positive charges are located in the TPSNF−PMMA layer in a region close to the SiO_2/TPSNF−PMMA interface. The nonhysteretic behavior of the $C-V_G$ curves of the "fresh" capacitor (Figure 2a) shows that these positive charges are immobile under the application of a −18 V/18 V forward/backward V_G sweep. The observed right shift of the $C-V_G$ curves with increasing irradiation time, in the case of low forward/backward V_G sweep (Figure 2b), indicates that UV irradiation reduces the number of positive trapped charges in the dielectric.

The motion of these positive charges depends on the strength and direction of the electric field in the gate dielectric. Figure 2c and d depict HF $C-V_G$ measurements after the application of high negative voltage stress (i.e., $V_{GS} = -25$ V for 1 min) to the "fresh" capacitor. Such a stressing voltage induces a remarkable flat-band voltage shift of 14.2 V toward the positive direction of the gate voltage (indicated by an arrow in Figure 2c), thus revealing a significant reduction in positive charge trapped at the SiO_2/TPSNF−PMMA interface. As a consequence of this charge reduction, subsequent UV irradiation causes a minimal right shift in the flat-band voltage of the nonhysteretic $C-V_G$ characteristics (see in Figure 2d the low forward/backward V_G sweep regions). It is important to note that the application of the above stress voltage does not alter the hysteretic behavior of the $C-V_G$ curves reported here above leading to similar flat-band voltage shifts (see Figure 2b, d) as a function of the applied V_G sweep amplitude and radiation dose. In addition, both capacitors (i.e., unstressed/stressed capacitors) exhibit identical $C-V_G$ and $V_{FB}-V_G$ characteristics (see inset in Figure 2d) for a prolonged irradiation time period of 50 min. These findings clearly

dx.doi.org/10.1021/am401016n | ACS Appl. Mater. Interfaces 2013, 5, 5667−5674

indicate that the hysteresis behavior of the $C-V_G$ curves originates from the motion of protons generated photochemically by subsequent irradiation of the TPSNF–PMMA dielectric layer.

Adsorption of Ph_3S^+ Cations on the SiO_2 Surface. The presence of positive charges trapped in the SiO_2/TPSNF–PMMA interface is attributed to the adsorption of Ph_3S^+ cations (of TPSNF salts) on the SiO_2 surface[32−35] during spin-coating of the TPSNF–PMMA solution in the polar solvent MIBK. The adsorption of Ph_3S^+ cations on the SiO_2 surface is expected to take place after the following equilibrium reactions (Scheme 2). Initially, the polar solvent MIBK is

Scheme 2. Mechanism of Adsorption of Ph_3S^+ Cations on the SiO_2 Surface during the Spin-Coating of TPSNF–PMMA Solution in the Polar Solvent MIBK

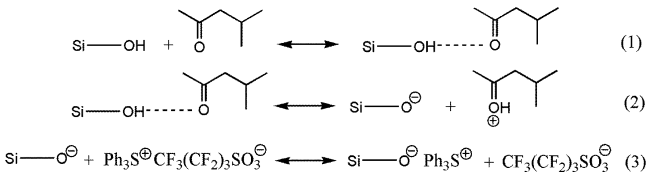

expected to be adsorbed on the SiO_2 surface through hydrogen bonding interactions with the silanol (Si–OH) groups that are known to exist on the SiO_2 surface (eq 1). Subsequently, the complex (SiOH···MIBK) formed is dissociated, leading to the formation of charged SiO^- sites on the SiO_2 surface (eq 2). Finally, the PH_3S^+ cations of the TPSNF salts interact with the charged SiO^- sites of the SiO_2 surface, where the sulfonate anions of the TPSNF salts are expected to be in the vicinity of Ph_3S^+ cations (eq 3). The interaction of Ph_3S^+ cations with polarized $SiO^{\delta-}$–$H^{\delta+}$ sites formed due to the polar solvent MIBK could be also possible, whereas the interaction of Ph_3S^+ cations with neutral Si–OH groups is considered rather unlikely.

In order to investigate the interaction of TPSNF salts (within TPSNF–PMMA films spin coated from the corresponding solutions in the polar solvent MIBK) with the SiO_2 surface, the decrease of TPSNF–PMMA film thickness caused by oxygen plasma was studied with FT-IR spectroscopy (Figure 4). The concentrations of TPSNF and PMMA were 20% w/w in polymer and 5% w/w in MIBK solution, respectively. The initial film thickness was 311 nm, and the etching rate was 1.4 nm s^{-1}. As shown in Figure 4a, increasing gradually the etching time up to 236 s the decreases of the following peaks were observed: (a) at 1732 cm^{-1} assigned to the C=O stretching vibration of PMMA and (b) at 1272 and 1242 cm^{-1} attributed to the asymmetric stretching of C–C–O coupled with C–O stretching of PMMA with a significant contribution to the 1272 cm^{-1} peak by the strong symmetric stretching of $S(=O)_2$ groups of TPSNF sulfonate anions at 1262 cm^{-1} (Figures 4b–d).[36,37] The contribution of the $S(=O)_2$ stretching (of TPSNF) to the 1272 cm^{-1} peak of PMMA is so significant that the absorption intensity ratio of the two peaks at 1271 and 1242 cm^{-1} (i.e., $r = A_{1271}/A_{1242}$) changes from $r < 1$ to $r > 1$ going from PMMA to the TPSNF–PMMA film (Figure 4b,d). The inset of Figure 4a shows that the decrease of the peaks at 1732 and 1272 cm^{-1} attributed to PMMA and both PMMA and TPSNF, respectively, is identical, indicating that the distribution of TPSNF salts within the TPSNF–PMMA film is uniform. It is interesting to observe that after 236 s of etching

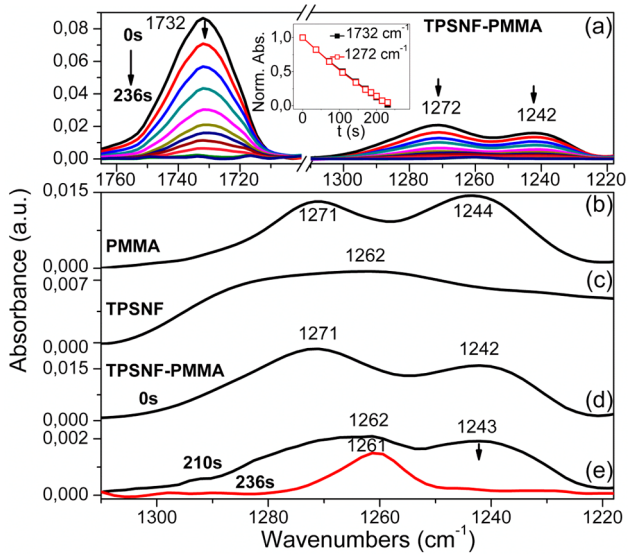

Figure 4. FT-IR spectra of (a, d, e) TPSNF–PMMA film (20% w/w in polymer and 5% in MIBK solution) during oxygen plasma etching at different times ranging from 0 to 236 s, (b) a PMMA film (5% w/w in MIBK solution), and (c) a TPSNF film (20 mg/mL in MIBK). Inset of a: change of the absorption intension of the FT-IR peaks of the TPSNF–PMMA film at 1732 cm^{-1} and 1272 cm^{-1} with the etching time.

the TPSNF–PMMA film, a peak at 1261 cm^{-1} attributed only to TPSNF salts appears, whereas the 1243 cm^{-1} peak assigned to PMMA completely disappears (Figure 4e). Consequently, a very thin (~5-nm-thick) TPSNF layer covers the SiO_2 surface after etching the TPSNF–PMMA film, giving clear evidence for the electrostatic interactions between TPSNF salts and SiO_2 surface. The fact that the remaining 1261 cm^{-1} peak is attributed to the sulfonate anions of TPSNF salts and not to their Ph_3S^+ cations does not oppose our initial hypothesis of interactions between the Ph_3S^+ cations and silanol groups of the SiO_2 surface, since the sulfonate anions of TPSNF salts are expected to be in the close vicinity of their counterions (Ph_3S^+).

A high negative voltage supplied to the gate electrode before irradiation, as discussed above, produces an electric field strong enough to move all or part of the interfacial cations (Ph_3S^+) toward the bulk of the TPSNF–PMMA layer, thus leading to a reduction of the negative flat-band voltage of the capacitor in agreement with the results depicted in Figure 2c,d. This correlates with the fact that upon irradiation of the "fresh" (i.e., the unstressed) capacitor, protons are generated by the photolysis of Ph_3S^+ cations causing a significant reduction in the concentration of Ph_3S^+ cations adsorbed on the SiO_2/TPSNF–PMMA interface.

The inset of Figure 5a shows the right shift of the nonhysteretic $C-V_G$ curves upon irradiation in the case of a low forward/backward V_G sweep for unstressed devices. The $C-V_G$ curves do not exhibit any right shift for prolonged irradiation times ($t_{pi} \geq 50$ min). A constant value of about 1.3 V (V_{FB}) was measured for the $C-V_G$ curves, indicating that the Ph_3S^+ cations adsorbed on the SiO_2 surface have vanished when the irradiation time (t_i) is greater than or equal to 50 min. The magnitude of the voltage shift, ΔV_{FB}, as a function of t_i is plotted in Figure 5a; here $\Delta V_{FB}(t_i) = V_{FB}(t_i) - V_{FB}(t_{pi})$ refers to the flat-band voltage difference between t_i and t_{pi} (3000 s). In the case of the "fresh" capacitor ($t_i = 0$ s), the absolute value of the voltage shift ($|\Delta V_{FB}(t_i = 0\ s)| = |\Delta V_{FB0}|$) is about 15.8 V,

dx.doi.org/10.1021/am401016n | ACS Appl. Mater. Interfaces 2013, 5, 5667–5674

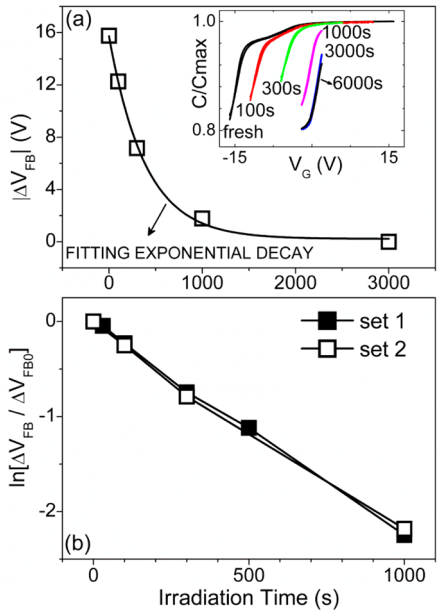

Figure 5. (a) Flat-band voltage shift of the nonhysteretic $C-V_G$ curves (inset) as a function of irradiation time. The solid line is a fitted exponential decay curve. (b) $\ln(|\Delta V_{FB}/\Delta V_{FB0}|)$ dependence as a function of the irradiation time. Sets 1 and 2 refer to two capacitors from different batches with identical processing conditions.

representing an effective surface density of adsorbed Ph_3S^+ cations at the SiO_2/TPSNF−PMMA interface of about 1.13×10^{12} cm^{-2}. An exponential decay curve fits well to the measured data, suggesting a linear fit of $\ln(|\Delta V_{FB}/\Delta V_{FB0}|)$ with the irradiation time as depicted in Figure 5b; sets 1 and 2 refer to two capacitors from different batches with identical processing conditions.

The disappearance of positive charge at the SiO_2/TPSNF−PMMA interface and the change in flat-band voltage of the MIS capacitor are well correlated with cumulative irradiation time. This observation is interesting in that it suggests another sensing scheme for the development of real-time radiation MIS-type sensors. Such a sensing scheme would be based on the aforementioned linear response of $\ln(|\Delta V_{FB}/\Delta V_{FB0}|)$ with a cumulative radiation dose in the case of low forward/backward V_G sweeps and not on the general concept discussed herein of mobile protons generated by irradiation in organic gate dielectrics, which lead to $C-V_G$ hysteresis phenomena under the application of high forward/backward V_G sweeps. It should be emphasized that while attractive the above alternative sensing scheme is associated with the magnitude of the flat-band voltage of the "fresh" capacitor which depends on parameters like the density of available silanol groups at the SiO_2 surface and the nature of the solvent used.

$C-V_G$ Behavior As a Function of the Solvent Used for the Preparation of the PAG-Containing Polymeric Gate Dielectric. Figure 6 depicts $C-V_G$ curves from two capacitors with TPSNF−PMMA (5/5% (w/w)) gate dielectrics of similar physical thickness that have been prepared using either MIBK (polar solvent) or toluene (nonpolar solvent). For the latter case, the "fresh" capacitor exhibits a much lower negative flat-band voltage, $V_{FB} = -5.9$ V (Figure 6b), in comparison to the MIBK case, $V_{FB} = -14.5$ V (Figure 6a). However, upon subsequent UV irradiation, both capacitors reveal comparable hysteresis loops; e.g., upon 1000 s UV irradiation and under the application of a forward (closed symbols)/backward (open

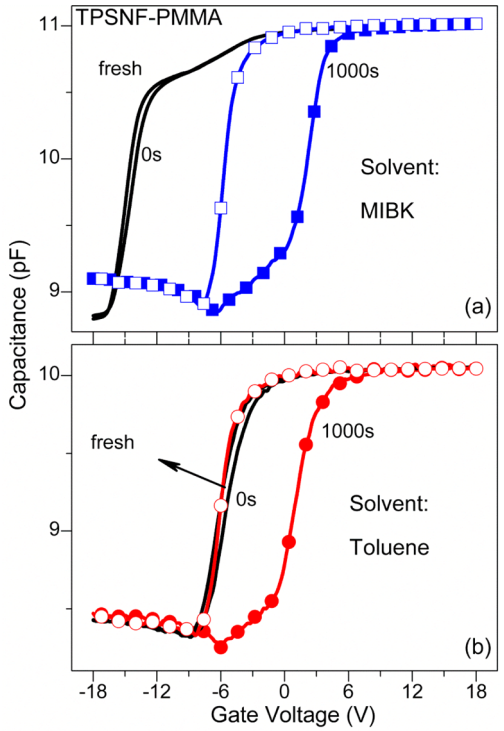

Figure 6. $C-V_G$ characteristics from two capacitors with TPSNF−PMMA (5/5% (w/w)) gate dielectrics of similar physical thickness that have been prepared using (a) MIBK solvent and (b) toluene solvent.

symbols) −18 V/18 V V_G sweep, the measured hysteresis loops for the two capacitors are 7.7 V and 7.1 V for MIBK (Figure 6a) and toluene (Figure 6b), respectively. This finding indicates that the number of mobile protons generated photochemically in the TPSNF−PMMA layer does not depend on the solvent used for the preparation of the PAG-containing polymeric gate dielectric.

The Effects of the $C-V_G$ Hysteresis Loops with TPSNF Concentration. Figure 7 illustrates the variation of the $C-V_G$ hysteresis loops (of the MIS structure shown in the inset of Figure 7c) and the corresponding flat-band voltage difference between forward and backward-stressed $C-V_G$ characteristics ($\Delta V_{FB}-V_G$ curves) with TPSNF concentration. All capacitors have TPSNF−PMMA layers comparable in physical thickness (∼ 270 nm) that are formed by spin coating of PMMA solutions containing TPSNF in various contents using MIBK as a solvent. For fabrication reasons, a 100-nm-thick PMMA isolation layer has been interposed between the semitransparent Al gate and the TPSNF/PMMA layer. The "fresh" capacitors (t = 0 s) do not exhibit any appreciable shift in the $C-V_G$ characteristics even at high gate voltages (inset of Figure 7a). However, with an increase in the TPSNF concentration, the flat-band voltage (V_{FB}) becomes more negative, thus indicating an increase in the effective surface density of the adsorbed Ph_3S^+ cations at the SiO_2/TPSNF−PMMA interface with TPSNF concentration. Furthermore, after subsequent irradiation and for a given forward/backward V_G sweep, ΔV_{FB} increases with increasing TPSNF concentration; e.g., for a −20/+20/−20 V V_G sweep, ΔV_{FB} is about 4.8 V, 7.0 V, and 14.6 V for the 5%, 10%, and 20% w/w cases, respectively, after an exposure time of 1000 s (Figure 7a). The $\Delta V_{FB}-V_G$ curves after UV exposure times of 300 and 1000 s are shown in Figure 7b and c, respectively. Interestingly, we

dx.doi.org/10.1021/am401016n | ACS Appl. Mater. Interfaces 2013, 5, 5667−5674

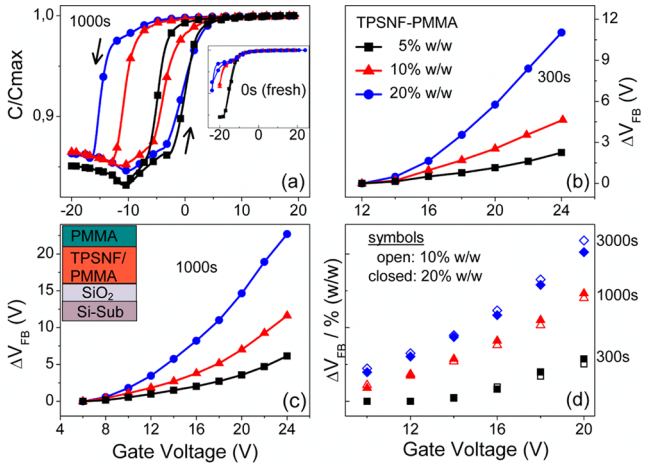

Figure 7. $C-V_G$ characteristics (a) and respective extracted flat-band voltage shifts (b and c) of MIS capacitors with a cross-section structure shown in c, inset, after exposure to UV light, as a function of the TPSNF content in the TPSNF–PMMA films (PMMA 5% w/w in MIBK solution, TPSNF in concentration 5%, 10%, and 20% w/w in polymer). The $C-V_G$ characteristics of nonirradiated unstressed (fresh) capacitors are shown in a, inset. (d) ΔV_{FB}/(TPSNF/PMMA % w/w) dependence on TPSNF concentration for the 10% and 20% w/w cases.

found that the ratio ΔV_{FB}/(TPSNF–PMMA % w/w) is independent of TPSNF concentration (see the results depicted in Figure 7d for the 10% and 20% w/w cases). Figure 8 shows

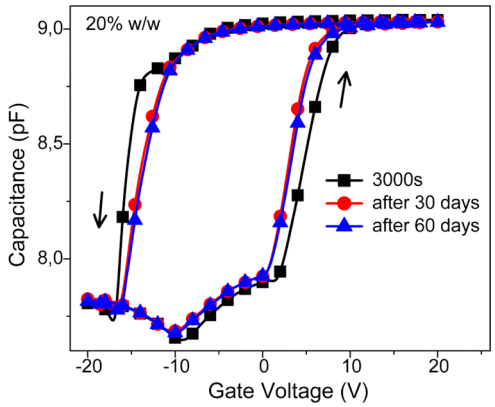

Figure 8. $C-V_G$ characteristics of Al/PMMA/TPSNF–PMMA/SiO_2/*n*-Si MIS capacitor with a TPSNF–PMMA film containing 20% w/w TPSNF after exposure to UV light and storage in the dark up to 60 days.

the $C-V_G$ curves of a capacitor with a TPSNF–PMMA gate dielectric containing 20% w/w TPSNF that were recorded after irradiation (3000 s) and different storage durations in the dark. After UV exposure, the flat-band voltage shift, ΔV_{FB}, was about 20.1 V. After one month storage duration, the ΔV_{FB} exhibits a slight decrease, from 20.1 to 17.1 V, and stabilizes thereafter (see the $C-V_G$ curve after two months following irradiation). These findings clearly reveal a nondestructive read-out operation of the MIS-type sensor.

The Effects of Gamma Irradiation on the $C-V_G$ Curves of the MIS Devices. The effect of gamma irradiation (^{60}Co) up to a dose of 10 kGy on the $C-V_G$ curves of MIS capacitors having a TPSNF–PMMA gate layer with various TPSNF concentrations has also been investigated at room temperature. Figure 9a shows $C-V_G$ characteristics for a −24/+24/−24 V V_G sweep after exposure to 10 kGy. The reference MIS device

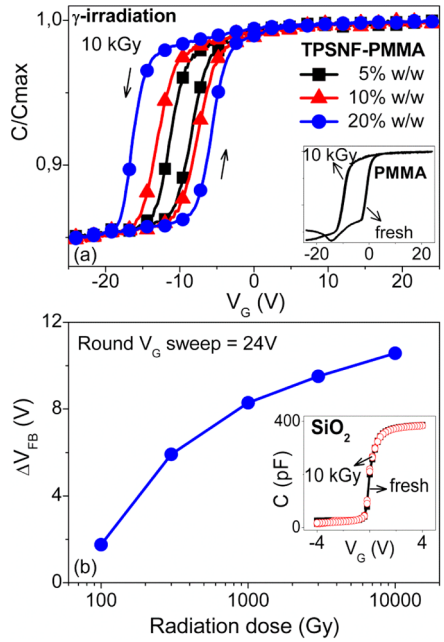

Figure 9. $C-V_G$ characteristics (a) and respective extracted flat-band voltage shifts (b) of Al/PMMA/(TPSNF/PMMA)/SiO_2/*n*-Si MIS capacitors irradiated up to an overall dose of 10 kGy. Inset a/b, $C-V$ curves of the reference MIS (Al/PMMA/SiO_2/*n*-Si)/MOS (Al/SiO_2/n-Si) capacitor before and after irradiation.

using a PMMA gate dielectric without TPSNF does not exhibit any appreciable $C-V_G$ hysteresis effect (see the inset in Figure 9a) but displays a significant negative V_{FB} shift (∼−8.5 V), which indicates that positive fixed charges have been created in the polymer film after gamma irradiation. We found that the V_{FB} shift and, thereby, the density of positive charges increase with the irradiation dose and probably relate to the rupture of chemical bonds at various places in the PMMA chain,[38] a trait that could be exploited for γ radiation dosimetry. The presence of such positive charges in the SiO_2 layer has been ruled out, as the reference MOS device does not exhibit any V_{FB} shift (see the inset in Figure 9b). A clear $C-V_G$ hysteresis effect is found for the 5, 10, and 20% w/w (TPSNF–PMMA) cases corresponding to a ΔV_{FB} of about 2.7, 5.5, and 10.6 V, respectively. These findings indicate that γ radiation induces a hysteresis loop in the $C-V_G$ curves with a magnitude proportional to the TPSNF concentration, as reported above in the case of UV exposure. Moreover, the hysteresis magnitude increases with the applied irradiation dose as depicted in Figure 9b, which shows the V_{FB} difference between forward (−24 V/24 V) and backward (24 V/−24 V)-stressed $C-V_G$ characteristics for an irradiation dose ranging from 0 to 10 kGy in the case of a capacitor using a TPSNF–PMMA gate dielectric with 20% w/w TPSNF. The above are encouraging to further development of real-time MIS-type sensors using organic gate dielectrics for the detection of γ rays.

3. CONCLUSIONS

In summary, we have explored the possibility of using photoacid-generator-(PAG)-containing polymeric films as the radiation-sensitive gate dielectrics of MIS-type dosimeters, wherein proton generation in those films as a function of the

ionizing radiation (IonR) dose is electronically sensed. Application of an electric field to the gate dielectric moves the protons and, thereby, alters the flat band voltage (V_{FB}) of the MIS device. The shift in the V_{FB} is proportional to the IonR-generated protons and, therefore, to the IonR total dose. We have shown that systematic improvements in sensitivity can be accomplished by increasing the concentration of the PAG molecules embedded in the polymeric matrix.

4. EXPERIMENTAL SECTION

Materials. Poly(methyl methacrylate) (PMMA, M_w = 350 000) was purchased from Du Pont. Triphenylsulfonium nonaflate (TPSNF) was obtained from Midori Kagaku. 1-(4′-(Dimethyl-aminophenyl)-6-phenyl-1,3,5-hexatriene (DMADPH) was obtained from Fluka. The solvents methyl isobutyl ketone (MIBK) and toluene were purchased from Aldrich. All chemicals used for MIS device fabrication were obtained from Merck.

Characterization Methods. UV−vis absorption spectra were obtained on quartz slides using a Perkin-Elmer UV−vis Lambda 40 spectrophotometer. Fourier transformed infrared (FT-IR) transmittance spectra at 4 cm^{-1} resolution, and 128 scans were obtained on Si wafers using a Bruker, Tensor 27 FT-IR spectrometer with a DTGS detector. The thicknesses of the photopolymeric films were measured using an Ambios Technology XP-2 profilometer. MIS devices were exposed either to deep UV light (using a DUV Orial Hg−Xe 600 W exposure tool; operated at 450 W) through a 249 nm narrow band (7 nm bandwidth at half-maximum) filter or to γ radiation using a ^{60}Co, 6500 Ci, gamma chamber. The dose rate provided by the γ radiation source is 6.67 Gy/min. The incident power of DUV radiation in the TPSNF−PMMA gate dielectric layer, through both the 249 nm filter and the semitransparent Al gate, was measured to be 2.42 $\mu W\ cm^{-2}$ (i.e., 72% reduced in comparison with the incident power through only the 249 nm filter; Figure 3 inset). The sample was irradiated for different doses by varying the time for irradiation. After each irradiation, the $C-V$ characteristics of the MIS capacitor were measured on a probe station using an HP4192A LCR meter at room temperature under normal atmospheric conditions.

Film Preparation. Solutions of PMMA in a concentration range of 3−5% w/w in MIBK and toluene were prepared. In the 5% w/w PMMA solutions, TPSNF in a concentration ranging from 5% to 20% w/w (in polymer) was added. In some of the TPSNF−PMMA solutions in MIBK with concentrations of 5% w/w in the polymer and 5% w/w in solution, respectively, the acid indicator DMA-DPH at a molar ratio of 1:1 in relation to TPSNF was added.

Device Fabrication. Si wafers were used as starting materials (⟨100⟩-oriented, n-type, 4-in., 5−10 Ω cm resistivity). A 500-nm-thick field oxide was first grown on the wafers using thermal oxidation. Then, square windows (300 μm edge length), which define the device active areas, were opened in the front side oxide using standard photolithography patterning and HF etching. SiO_2 on the back side of the wafers was etched away during this procedure. After resist removal and cleaning, the wafers were thermally oxidized (900 °C in dry oxygen) for the purpose of forming a SiO_2 film (7.5 nm in thickness) in the device active areas. A TPSNF−PMMA film was then formed on the oxide-coated active areas by spin-coating (at 3000 rpm) of the corresponding polymeric solutions and then thermally treated at 150 °C for 60 min (film thickness ∼270 nm). In a few cases, a thin (100-nm-thick) PMMA film was spin coated under similar conditions on top of the TPSNF−PMMA layer. After polymeric film preparation, a thin (∼12-nm-thick) aluminum layer was deposited onto the front side of the samples by electron-beam evaporation, and contact pads (400 × 400 μm^2) were defined on the top of the active areas and the surrounding field oxide using photolithography patterning and Al etching. Photoresist material onto the Al contact pads was removed by oxygen plasma etching. The above process ensured the "encapsulation" of the sensitive polymeric films and resulted in their longevity, robustness, and high yields. Device fabrication was completed by etching away SiO_2 from the wafer back side, forming aluminum substrate contact (500-nm-thick), and finally annealing the samples at 120 °C for 15 min.

The above film preparation conditions were applied in the present work, except for the case of use of an acid indicator DMA-DPH within the TPSNF−PMMA films, where the films were thermally treated at a lower temperature (110 °C, 1 min) in order to prevent the removal of the indicator from the film.

AUTHOR INFORMATION

Corresponding Author

*E-mail address: ekapetan@chania.teicrete.gr.

Notes

The authors declare no competing financial interest.

ACKNOWLEDGMENTS

We thank Dr. Kyriakos Papadopoulos in the Department of Physical Chemistry, NCSR "Demokritos" for the γ radiation experiment. This research has been cofinanced by the European Union (European Social Fund—ESF) and Greek national funds through the Operational Program "Education and Lifelong Learning" of the National Strategic Reference Framework (NSRF)—Research Funding Program: ARCHIMEDES III. Investing in knowledge society through the European Social Fund.

REFERENCES

(1) Knoll, G. F. In *Radiation Detection and Measurement*; Wiley: New York, 2000.
(2) Holmes-Siedle, A. *Nucl. Instrum. Methods* **1974**, *121*, 169−179.
(3) Holmes-Siedle, A.; Adams, L. *Radiat. Phys. Chem.* **1986**, *28* (2), 235−244.
(4) Sarrabayrouse, G.; Siskos, S. *IEEE Instr. Meas. Mag.* **1998**, *1* (3), 26−34.
(5) Barthe, J. *Nucl. Instrum. Methods B* **2001**, *184*, 158−189.
(6) Rosenfeld, A. B. *Radiat. Meas.* **2007**, *41*, S134−S153.
(7) Oldham, T. R.; McLean, F. B. *IEEE Trans. Nucl. Sci.* **2003**, *50*, 483−499.
(8) Arshak, K.; Korostynska, O. *IEEE Sens. J.* **2005**, *5*, 574−580.
(9) Senthil Srinivasan, V. S.; Pandya, A. *Thin Solid Films* **2011**, *520*, 574−577.
(10) Maleki, T.; Ziaie, B. *IEEE Electron Device Lett.* **2010**, *31*, 767−769.
(11) Lima Pacheco, A. P.; Araujo, E. S.; de Azevedo, W. M. *Mater. Charact.* **2003**, *50*, 245−248.
(12) Raval, H. N.; Tiwari, S. P.; Navan, R. R.; Rao, V. R. *Appl. Phys. Lett.* **2009**, *94*, 123304−123304-3.
(13) Blakesley, J. C.; Keivanidis, P. E.; Campoy-Quiles, M.; Newman, C. R.; Jin, Y.; Speller, R.; Sirringhaus, H.; Greenham, N. C.; Nelson, J.; Stavrinou, P. *Nucl. Instrum. Methods A* **2007**, *580*, 774−777.
(14) Lavery, L. L.; Whiting, G. L.; Arias, A. C. *Org. Electron.* **2011**, *12*, 682−685.
(15) Ma, J.; Yeowa, J. T. W.; Chow, J. C. L.; Barnett, R. B. *Carbon* **2008**, *46*, 1869−1873.
(16) Gao, X.; Kang, Q. S.; Yeow, J. T. W.; Barnett, R. *Nanotechnology* **2010**, *21*, 285502−8.
(17) Lobez, J. M.; Swager, T. M. *Angew. Chem., Int. Ed.* **2010**, *49*, 95−98.
(18) Ahmadi, M.; Yeow, J. T. W. *Biosens. Bioelectron.* **2011**, *26*, 2171−2176.
(19) Hana, J.-W.; Meyyappan, M.; Ahn, J.-H.; Choi, Y.-K. *Sens. Actuators, A* **2012**, *182*, 1−5.
(20) Tokita, S.; Watanabe, F.; Hashimoto, K.; Tachikawa, T. *J. Photopolym. Sci. Technol.* **2001**, *14*, 221−224.
(21) Tachikawa, T.; Naito, M. *J. Photopolym. Sci. Technol.* **2004**, *17*, 81−86.
(22) Kapetanakis, E.; Douvas, A. M.; Velessiotis, D.; Makarona, E.; Argitis, P.; Glezos, N.; Normand, P. *Adv. Mater.* **2008**, *20*, 4568−4574.

(23) Crivello, J. V.; Lam, J. H. W. *J. Polym. Sci., Polym. Chem.* **1979**, *17*, 977−999.
(24) Dektar, J. L.; Hacker, N. P. *J. Am. Chem. Soc.* **1990**, *112*, 6004−6015.
(25) Kozawa, T.; Tagawa, S. *Jpn. J. Appl. Phys.* **2010**, *49*, 030001−19.
(26) Stewart, K. J.; Hatzakis, M.; Shaw, J. M.; Seeger, D. E.; Neumann, E. *J. Vac. Sci. Technol. B* **1989**, *7*, 1734−1739.
(27) Gather, M. C.; Kohnen, A.; Falcou, A.; Becker, H.; Meerholz, K. *Adv. Funct. Mater.* **2007**, *17*, 191−200.
(28) Georgiadou, D. G.; Palilis, L. C.; Vasilopoulou, M.; Pistolis, G.; Dimotikali, D.; Argitis, P. *J. Mater. Chem.* **2011**, *21*, 9296−9301.
(29) Pistolis, G.; Boyatzis, S.; Chatzichristidi, M.; Argitis, P. *Chem. Mater.* **2002**, *14*, 790−796.
(30) Veres, J.; Ogier, S.; Lloyd, G.; de Leeuw, D. *Chem. Mater.* **2004**, *16*, 4543−4555.
(31) Schroder, D. K. In *Semiconductor Material and Device Characterization*; Wiley-Interscience: New York, 1998; Ch. 6.
(32) Ong, S.; Zhao, X.; Eisenthal, K. B. *Chem. Phys. Lett.* **1992**, *191*, 327−335.
(33) Dong, Y.; Pappu, S. V.; Xu, Z. *Anal. Chem.* **1998**, *70*, 4730−4735.
(34) Xu, Z.; Li, J.; Dong, Y. *Langmuir* **1998**, *14*, 1183−1188.
(35) Van Tilborg, W. J. M. *Tetrahedron* **1975**, *31*, 2841−2844.
(36) O'Reilly, J. M.; Mosher, R. A. *Macromolecules* **1981**, *14*, 602−608.
(37) Silverstein, R. M.; Bassler, G. C.; Morrill, T. C. In *Spectroscopic Identification of Organic Compounds*, 4th ed.; John Wiley & Sons: New York, 1981.
(38) Todd, A. *J. Polym. Sci.* **1960**, *42*, 223−247.